Theoretical Estimation of Segmental Orientation in Deformed Polymeric Networks Using a Lattice Model and Application to Orientation of Amorphous Chain Segments of Poly(ethylene terephthalate) and Oriented Crystallization of Polyethylene

Masaru Matsuo,*,† Junko Ooki,† Yuuko Harashina,† Tetsuya Ogita,‡ and R. St. John Manley§

Department of Textile and Apparel Science, Faculty of Human Life and Environment, Nara Women's University, Nara 630, Japan, Department of Materials Science and Engineering, Faculty of Engineering, Yamagata University, Yonezawa 992, Japan, and Department of Chemistry, McGill University, Montreal H3A 2A7, Canada

Received November 15, 1994; Revised Manuscript Received April 3, 1995®

ABSTRACT: The orientation distribution of chain segments in a uniaxially deformed polymer film has been estimated theoretically as a function of draw ratio using a lattice model similar to the one proposed by Erman et al. The model of Erman et al. was somewhat modified to compare the theoretical results with experimental ones. In doing so, the preferred axis associated with the orientation of segments was chosen along the direction between the two successive cross-link points, and the orientation of the preferred axis was assumed to behave in an affine fashion under elongation. The treatment was formulated in terms of the orientation distribution function with respect to the stretching direction by the application of the Legendre addition theorem. Numerical calculations were carried out to study the mechanism of the orientation of amorphous chain segments of poly(ethylene terephthalate) (PET) films, as well as oriented crystallization of polyethylene (PE) films. X-ray diffraction measurements were done to obtain the orientation distribution functions for PET and PE drawn films. The calculated orientation distribution functions were in good agreement with those observed experimentally.

Introduction

Segmental orientation in uniaxially deformed elastomatic networks has been treated in terms of gaslike theories and liquidlike theories.[1-4] In the gaslike theories the chain vector and segment vector distributions have been estimated theoretically by using idealized models in which the effects of mutual interference between chain segments are neglected.

In an attempt to improve the gaslike theory, the effect of intermolecular interferences relating to orientation-dependent packing entropy was taken into consideration by Di Marzio in a liquidlike theory based on a lattice model.[3] In the theory, Di Marzio derived a negative correction term to the stress–strain curves of the gaslike theory. He showed that, on stretching a network, the segments tend to order along the stretching direction in order to decrease the mutual interference between them. Tanaka and Allen solved the problem self-constantly.[4] They found a negative contribution to the stress–strain relation, which is twice as large as Di Marzio's estimation.

In the lattice models of Di Marzio and Tanaka and Allen, the effect of chain stiffness on segmental orientation was not considered. In a recent paper, Erman et al.[5,6] have attempted to improve the liquidlike theory in this direction. For this purpose they adopted the lattice theory of Flory[7,8] for chains with freely jointed rodlike segments and applied it to a thermotropic system with anisotropic polarizabilities. Their treatments[5,6] are of interest to understand the detailed phenomena of molecular orientation of actual polymeric materials under elongation. In their model system, the length-to-width ratio x of each segment of a chain, which is a measure of chain stiffness, is incorporated into the theory of segmental orientation. Namely, Erman et al. pointed out that a segment of a polyethylene chain with 10–22 bonds may be viewed as a rodlike object on the basis of the concept of Flory and Yoon that a more rigorous analysis of the equivalent segment size of a freely jointed chain for polyethylene by matching the higher order moments of the end-to-end distance of the real and the freely jointed chain leads to $m_r/m \doteq 20-22$ (m_r = the number of segments in a real chain and m = the number of Kuhn segments).[9] They introduced intermolecular contributions in networks with flexible chains as well as thermotropic effects between segments which result in phase transitions due to orientation upon stretching and formulated the second-order orientation factor associated with the second term of the Legendre function.

However, a question arises as to why the second-order orientation factor calculated by Erman et al. assumes a positive value even in an undrawn state ($\lambda = 1$) at larger values of x.[5] This phenomenon has never been observed for polymer films, and the value of the orientation factor for $\lambda = 1$ must be obviously zero, indicating a random orientation of molecular segments. However, their concept is essentially correct in terms of the Helmholtz free energy. Actually, except for films, it is well-known that beyond a critical axial ratio x_c, systems of rodlike particles spontaneously split into two phases with different anisotropy, since the existing entropic driving forces are supplemented by an orientation-dependent energetic contribution. To explain this phenomenon, Flory et al. have taken the preferred axis of a given domain along one of the principal axes of the lattice for liquid crystal systems and of hard rods dispersed in a dilute solution.[7,8] Based on the same concept, the stretching direction for the model of Erman

* To whom all correspondence should be addressed.
† Nara Women's University.
‡ Yamagata University.
§ McGill University.
® Abstract published in *Advance ACS Abstracts,* June 1, 1995.

0024-9297/95/2228-4951$09.00/0

et al.[5,6] is chosen as the preferred direction which allows the preferential orientation of a segment. This leads to an abnormal phenomenon where polymer chains within a film are oriented without elongation in order to minimize the free energy. In the present paper, a modified model is proposed to solve this contradiction for polymer films, in which the preferred axis is chosen along the direction between two successive cross-link points. This modified model is employed to analyze the orientation distribution of amorphous chain segments of poly(ethylene terephthalate) (PET) and orientation of crystallites of polyethylene (PE) during the process of oriented crystallization. The actual estimation of amorphous chain segments was done in terms of the orientation distribution function instead of the second-order orientation factor.

Experimental Section

Amorphous PET films with a thickness of 500 μm were obtained by casting from solutions in *o*-chlorophenol. The average molecular weight was obtained from viscosity measurements using *o*-chlorophenol at 30 °C. The samples with a random orientation of amorphous chain segments were cut into strips of 70 × 15 mm which were used to investigate the orientation of amorphous chain segments by elongation. Elongation was done in a hot water bath at 90 °C; each specimen was preheated at the same temperature and stretched to the desired elongation ratio. Immediately following the stretching, the stretcher with the sample was quenched to room temperature.[10] The sample was removed from the stretcher after 10 min. The densities of the films were measured by a pycnometer using a mixture of *n*-heptane and carbon tetrachloride as a medium. The degree of crystallinity was calculated by assuming the densities of the crystalline and amorphous regions to be 1.445 and 1.335 g cm^{-3}, respectively.[11]

A linear polyethylene with a viscosity-average molecular weight $\bar{M}_v = 70\,000$ was used to prepare two kinds of PE films by calendering methods. Melt PE was calendered under rolls at 65 and 125 °C, respectively. The draw ratio of the calendered films was determined from the friction ratio of the rolls. The draw ratios, λ, of the films were 1.5 and 4.0, respectively. The crystallinity of the films was calculated from the density which was measured by a pycnometer in chlorobenzene−toluene as a medium, by assuming densities of the crystalline and amorphous phases to be 1.000 and 0.852 g cm^{-3}, respectively.[12] The crystallinities of the films with λ = 1.5 and 4.0 were 69.2 and 70.6%, respectively. The corresponding melting points were 130 and 133 °C, respectively, which were estimated from the melting endotherms of differential calorimetry (DSC) curves obtained at a constant rate of 10 °C min^{-1}. Young's moduli of the specimens were 1.6 and 2.7 GPa, respectively, at 20 °C. Incidentally, polarized H_v light scattering patterns indicated the existence of rodlike textures.

The X-ray measurements were carried out using a 12-kW rotating-anode X-ray generator (Rigaku RAD-rA). The intensity distribution was measured with point focusing using a system in which the incident beam was collimated by a collimator 2 mm in diameter and the diffraction beam was detected by a slit 0.9 × 0.9 mm.[13] The incident beam was monochromatized by a curved graphite monochromator. The intensity distribution was measured with a step-scanning device at a step interval of 0.1°, each at a fixed time of 40 s, in the desired range of diffraction angles. Incidentally, when the incident beam was directed parallel to the stretching direction (end view), the diffraction patterns of both the specimens show circular diffraction rings indicating a random orientation of crystallites with respect to the stretching direction.

Theory

To facilitate understanding of the difference between the model of Erman et al.[5,6] and the present concept, we shall refer to the geometrical arrangements to explain segmental orientation. For this purpose, efforts have been made to preserve the notation used by Erman et al. as much as possible. For simplicity, the network chains will be assumed to be monodisperse, i.e., composed of the same number m of rods having an identical axial ratio x. The lateral dimensions of the rods will be of the size of solvent molecules or lattice sites. Figure 1a shows an illustrative network chain consisting of Kuhn segments (i.e., freely jointed rods) between two successive cross-link points. The U_3 axis parallel to the direction between the two cross-link points is specified with respect to the Cartesian coordinate $0-X_1X_2X_3$ within the space of the film, the X_3 axis being along the stretching direction and the X_2X_3 plane being parallel to the surface of the film, in which Θ is the polar angle between the U_3 and X_3 axes. In Figure 1b, the V axis denoting the direction of a given segment of a network chain is defined by the polar angle θ and the azimuthal angle ϕ with respect to the Cartesian coordinate $0-X_1X_2X_3$. The orientation of the segment is specified by the polar angle Ψ and the azimuthal angle Φ with respect to the Cartesian coordinate $0-U_1U_2U_3$ as shown in Figure 1c, in which the U_1 and U_2 axes are chosen arbitrarily in the plane perpendicular to the U_3 axis. Following Flory et al.,[8] the accommodation of the rod in the lattice is achieved through its representation by a sequence of $y_k = x \sin \Psi_k$ submolecules, each occupying x/y_k sites and oriented along the preferred direction, U_3 axis, as shown in Figure 1d. Thus, y_k characterizes the given rod. It is expressed in terms of Ψ_k and Φ_k as[8]

$$y_k = x \sin \Psi_k(|\cos \Phi_k| + |\sin \Phi_k|) \qquad (1)$$

for the rod exhibiting that particular orientation. Accordingly, the value of y_k increases as the rod becomes disoriented, as pointed out by Erman et al.[5,6] In the model system proposed by Erman et al., the preferred direction corresponds to the stretching direction (X_3 axis), while in the present model system, the preferred direction is taken along the U_3 axis denoting the direction between the two successive cross-link points as shown in Figure 1a. According to the model proposed

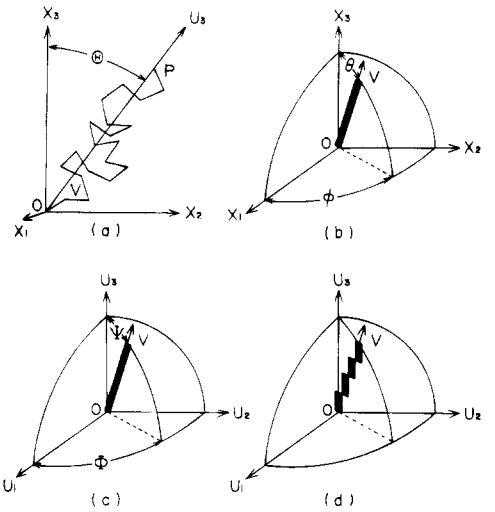

Figure 1. (a) Network chains of Kuhn segments between the two successive cross-link points O and P. (b) Diagram illustrating the polar and azimuthal angles θ and ϕ, which specify the orientation of a segment of a chain with respect to Cartesian coordinate $0-X_1X_2X_3$ fixed within the film space. (c) Polar angle Ψ and azimuthal angle Φ specify the orientation of a segment of a chain with respect to the Cartesian coordinate $0-U_1U_2U_3$. (d) Division of the segment into $y_k = x \sin \Psi_k$ submolecules, each oriented along the preferred direction.

by Erman et al., the rods orient to the stretching direction without elongation in order to minimize the free energy of a given system, when the length-to-width ratio x of the Kuhn segment is beyond the critical value. Considering the Helmholtz free energy, this is undoubtedly reasonable for highly ordered chains to form a liquid crystal system and for highly oriented hard rods dispersed in a dilute solution. In spite of the rigorous treatment for the above systems in terms of the Helmholtz free energy, such a preferential orientation has never been observed for polymer films. To avoid this contradiction, the preferred axis is chosen along the direction between the two cross-link points. This treatment is similar to that of freely jointed chains of finite length represented by the distribution of Langevin.

Since y_k characterizes the spatial orientation of a given rod and is referred to as its disorientation index, the mean disorientation index, y, for the system of n_2 chains is defined by

$$y = \frac{1}{n_2 m}\sum_{l=1}^{n_2}\sum_{k} n_{l,k} y_k \tag{2}$$

where $n_{l,k}$ indicates the number of segments of the lth chain, whose orientation lies within the kth solid angle.

The total configurational partition function of a system of n_2 polymer and n_1 solvent molecules in a lattice consisting of n_0 sites ($n_0 = n_1 + mxn_2$) can be given by $Z_m = Z_{comb}Z_{orient}$, where Z_{comb} and Z_{orient} are the combinational part and orientational part of the partial function. The configuration partition function Z_m is used in the evaluation of the Helmholtz free energy change of mixing according to

$$\Delta A_m = -k_B T \ln Z_m \tag{3}$$

where k_B is the Boltzmann constant and T is the absolute temperature. According to Erman et al.,[5] $-\ln Z_{comb}$ is given by

$$-\ln Z_{comb} = n_1 \ln v_1 + n_2 \ln(v_2/mx) - (n_1 + n_2 my)\ln[1 - v_2(1 - y/mx)] + n_2(my - 1) - n_2(m - 1)\ln(z - 1) \tag{4}$$

where v_2 is a volume fraction of polymer given as mxn_2/n_0.

On the other hand, the orientational partition function Z_{orient} is given by

$$Z_{orient} = \prod_{j=1}^{n_2} m! \prod \frac{\omega_k^{n_{j,k}}}{n_{j,k}!} = \prod_{j=1}^{n_2} (\sum n_{j,k})! \prod_k \frac{\omega_k^{n_{j,k}}}{n_{j,k}!} \tag{5}$$

where ω_k is the kth fractional range of the solid angle replaced by $(1/4\pi)\sin\Psi_k\, d\Psi_k$. Here it is evident that an equilibrium distribution of segments among different orientations is obtained by minimizing the free energy of the system with respect to $n_{j,k}$ to find the distribution of the probabilities of different configurations of segments in the network between the two cross-link points. The imposition of external constraints requires the use of Lagrange multipliers to minimize the free energy. Thus,

$$\frac{\partial}{\partial n_{j,k}}[\ln Z_m] = 0 \tag{6}$$

$$\sum n_{j,k} = m \tag{7}$$

$$\sum n_{j,k} \cos\Psi_k b = h \tag{8}$$

where b is the length of a segment and h is the distance between the two cross-link points. From eqs 7 and 8, we have

$$\alpha \sum \delta n_{j,k} = 0 \tag{9}$$

$$\beta \sum \cos\Psi_k\, \delta n_{j,k} = 0 \tag{10}$$

Substituting eqs 9 and 10 into eq 6, it takes the form

$$n_{j,k}/m\omega_k = \exp(\beta\cos\Psi_k - \alpha y_k - 1) \tag{11}$$

where

$$\alpha = -\ln[1 - v_2(1 - y/x)] \tag{12}$$

Thus, the distribution of eq 11 reduces to

$$n_{j,k}/m = (1/4\pi)\exp(\beta\cos\Psi_k - \alpha y_k - 1)\sin\Psi_k\, d\Psi_k \tag{13}$$

Considering the difficulty in carrying out a double integration to determing β, the problem can be simplified to a considerable extent by preaveraging the Φ dependence prior to numerical integration over Ψ.[6,8] Accordingly,

$$y_k = (4x/\pi)\sin\Psi_k \tag{14}$$

When eq 13 is used and summations over directions are replaced by integrals, the conditions imposed by the constraints may be written as

$$(1/2)\int_0^\pi \exp[\beta\cos\Psi_k - (4x\alpha/\pi)\sin\Psi_k - 1]\sin\Psi_k\, d\Psi_k = 1 \tag{15}$$

and

$$(bm/2)\int_0^\pi \exp[\beta\cos\Psi_k - (4x\alpha/\pi)\sin\Psi_k - 1]\cos\Psi_k \sin\Psi_k\, d\Psi_k = h \tag{16}$$

From eqs 15 and 16, we obtain

$$h/bm = \frac{\int_0^\pi \exp[\beta\cos\Psi_k - (4x\alpha/\pi)\sin\Psi_k]\cos\Psi_k \sin\Psi_k\, d\Psi_k}{\int_0^\pi \exp[\beta\cos\Psi_k - (4x\alpha/\pi)\sin\Psi_k]\sin\Psi_k\, d\Psi_k} \tag{17}$$

Thus, the orientation distribution function can be represented by omitting the dummy subscript k as follows:

$$f(\Psi) = Q_0 \exp[\beta\cos\Psi - (4x\alpha/\pi)\sin\Psi] \tag{18}$$

where Q_0 is a normalized constant given by

$$Q_0 = 1/\int_0^\pi \exp[\beta\cos\Psi - (4x\alpha/\pi)\sin\Psi]\sin\Psi\, d\Psi \tag{19}$$

By expanding both the numerator and denominator in eq 17 into the Taylor series and keeping only the linear term of α and β, eq 17 reduces to

$$h/bm = \beta/3(1 - ax) \tag{20}$$

To calculate y/x according to the method by Erman et al.,[5] we have

$$y = \frac{\int_0^\pi (4x/\pi) \sin \Psi \exp[\beta \cos \Psi - (4xa/\pi) \sin \Psi] \sin \Psi \, d\Psi}{\int_0^\pi \exp[\beta \cos \Psi - (4xa/\pi) \sin \Psi] \sin \Psi \, d\Psi} \tag{21}$$

By expanding the exponential part of both the numerator and the denominator in eq 21 up to second order in a and β, we have

$$y/x = \frac{1 - (32ax/3\pi^2) + (\beta^2/8) + (2a^2x^2/\pi^2)}{1 - ax + (1/6)\beta^2 + (16a^2x^2/3\pi^2)} = 1 + ax\{1 - (32/3\pi^2)\} - \beta^2/24 \tag{22}$$

Using the approximation, we have

$$a = -\ln[1 - v_2(1 - y/x)] = v_2(1 - y/x) \tag{23}$$

From eqs 22 and 23, we have

$$a = \frac{1}{2x}\{(2 + d/x) - (d/x)^2 + 4(d/x)\} \tag{24}$$

where

$$d = 24\left\{1 - \frac{xv_2}{x_2}\right\} m^2 b^2/9v^2h^2 \tag{25}$$

and

$$x_a = 1/\{(32/3\pi^2) - 1\} \tag{26}$$

For freely jointed chains under affine deformation, the root-mean-square vector distance h_0 in the free state is related to

$$h_0 = mb^2 \tag{27}$$

When the sample is stretched to a draw ratio λ, the length h of the segment with the end-to-end vector of length h_0 in the direciton Θ in Figure 1a becomes

$$h = h_0\lambda/\{\lambda^3 - (\lambda^3 - 1)\cos^2 \Theta\}^{1/2} \tag{28}$$

Thus, the orientation distribution function of the end-to-end vectors between the two cross-link points becomes

$$g(\Theta) = (\lambda^3/2)/\{\lambda^3 - (\lambda^3 - 1)\cos^2 \Theta\}^{3/2} \tag{29}$$

For further development, it is convenient to have $f(\Psi)$ (see eq 18) expanded in a series of spherical harmonics, i.e.,[14-16]

$$f(\Psi) = \sum_{l=0} C_{l00}\Pi_l(\cos \Psi) \tag{30}$$

and

$$C_{l00} = \int_{-1}^{1} f(\Psi)\Pi_l(\cos \Psi) \, d(\cos \Psi) \tag{31}$$

where $\Pi_l(x)$ is the normalized Legendre polynominal.

For numerical calculations, $f(\Psi)$ is expanded into the Taylor series up to the seventh order.

$$f(\Psi) = Q_0 \exp[\beta \cos \Psi - (4xa/\pi) \sin \Psi] = Q_0 \exp(Y)$$
$$= Q_0\{1 + Y + (1/2)Y^2 + (1/6)Y^3 + (1/24)Y^4 + (1/120)Y^5 + (1/720)Y^6\} \tag{32}$$

Here we shall define the orientation distribution function $\omega_{am}(\cos \theta)$ of segments with respect to the Cartesian coordinate $0\text{-}X_1X_2X_3$. The function can be represented as a series of Legendre polynominals, i.e.,

$$\omega_{am}(\cos \theta) = \sum_{l=0}^{\infty} A_{l00}\Pi_l(\cos \Psi) \tag{33}$$

with

$$A_{l00} = \int_{-1}^{1} \omega_{am}(\cos \theta)\Pi_l(\cos \theta) \, d(\cos \theta) \tag{34}$$

Considering the geometrical arrangement in Figure 1a–c, the angle θ between a segment and the stretching direction is related to Ψ, Φ, and Θ by

$$\cos \theta = \cos \Psi \cos \Theta + \sin \Psi \sin \Theta \cos \Phi \tag{35}$$

Application of the Legendre addition theorem to eq 35 led to

$$\Pi_l(\cos \theta) = \left\{\left(\frac{2}{2l + 1}\right)^{1/2} \sum_{m=-l}^{l} \Pi_l^m(\cos \Theta)\Pi_l^m(\cos \Psi) \exp(-im\Phi)\right\} \tag{36}$$

From eq 34, it is seen that the coefficient A_{l00} is the average value of $\Pi_l(\cos \theta)$ for the segments. Therefore, A_{l00} is obtained if we multiply both sides of eq 36 by the orientation distribution functions, $\omega_{am}(\cos \theta)$, $g(\Theta)$, and $f(\Psi,\Phi)$ and integrate over the whole range of θ, Θ, Ψ, and Φ. Hence,

$$A_{l00} = \left(\frac{2}{2l + 1}\right)^{1/2} \sum_{m=-l}^{l} \int_0^{2\pi} \int_{-1}^{1} \Pi_l^m(\cos \Theta)\Pi_l^m(\cos \Psi) \exp(-im\Phi) \, g(\Theta) \, f(\Psi,\Phi) \, d\Theta \, d(\cos \Psi) \, d\Phi$$
$$= \left(\frac{2}{2l + 1}\right)^{1/2} \sum_{m=-l}^{l} \int_0^{\pi} 2\pi \left[\frac{1}{2\pi} \int_0^{2\pi} \int_{-1}^{1} f(\Psi,\Phi) \, \Pi_l^m(\cos \Psi) \exp(-im\Phi) \, d(\cos \Psi) \, d\Phi\right] \Pi_l^m(\cos \Theta) g(\Theta) \, d\Theta$$
$$= 2\pi\left(\frac{2}{2l + 1}\right)^{1/2} \int_{-1}^{1} C_{l00} \, g(\Theta) \, \Pi_l^m(\cos \Theta) g(\Theta) \, d\Theta \tag{37}$$

Here, l and m are even integers. The normalized associated Legendre's polynominal $\Pi_l^m(\cos Y)$ and coefficient A_{l00} can be related to the associated Legendre's polynominal $P_l^m(\cos Y)$ and the coefficient F_{l00} as follows:[17,18]

$$P_l^m(\cos Y) = \left(\frac{2}{2l + 1}\right)^{1/2} \Pi_l^m(\cos Y) \tag{38}$$

and

$$F_{l00} = \left(\frac{2}{2l+1}\right)^{1/2} 4\pi^2 A_{l00} \quad (39)$$

Substituting eqs 38 and 39 into eq 33, we have

$$4\pi^2 \omega_{am}(\cos\theta) = {}^1/_2 + 2\sum_{l=2}^{\infty} \frac{2l+1}{2} F_{l00} P_l(\cos\theta) \quad (40)$$

The actual calculation for orientation distribution of amorphous chain segments was carried out by using eq 40.

According to Bahar et al.,[8] the lattice model of segmental orientation can be applied to the thermotropic system with anisotropic polarizabilities. The treatment was first proposed by Flory[8] for thermotropic systems with orientation-dependent interaction, and the theory is useful to explain the transition between crystalline, nematic, and isotropic phases for several specimens such as poly(*p*-phenylenes). The theory contains a factor of energetic character which contributes to a first-order transition from a relatively disordered to a highly oriented structure, upon imposition of an external perturbation. In this case, the new orientation distribution function $f_t(\Psi)$ can be written as

$$f_t(\Psi) = Q_0 \exp[\beta \cos\Psi - (4xa/\pi)\sin\Psi + ST^{-1}P_2(\cos\Psi)] \quad (41)$$

where

$$S = \int_0^\pi f_t(\Psi) P_2(\cos\Psi) \sin\Psi \, d\Psi / \int_0^\pi f_t(\Psi) \sin\Psi \, d\Psi \quad (42)$$

In eq 41, T is given by

$$T = \frac{k_B T}{x}\left[\frac{Cz_c(\Delta\alpha)^2}{r_*^6}\right]^{-1} \quad (43)$$

where z_c is the number of first neighbors surrounding the segment, $\Delta\alpha$ is the mean anisotropy of all segments, r_* is the distance between subsegments for dense packing, and C is a constant.

By using a derivation similar to eqs 22–24, a is given by

$$a = \frac{1}{2x}\{2 - D/U - (D/U)^2 - (4D/U)\} \quad (44)$$

where

$$D = (dx/8) - dd_0(1 - T/5) \quad (45)$$

$$U = \{d_0(1 - T/5) + 9dh^2/15m^2b^2\}x \quad (46)$$

$$d_0 = 8\left(1 - \frac{xv_2}{x_a}\right)/Tv_2 \quad (47)$$

Using the same treatment as shown in eqs 21 and 22, we have

$$y/x = 1 + ax\{1 - (32/3\pi^2)\} - \beta^2/24 - ST^{-1}/8 \quad (48)$$

From eq 42, we also obtain

$$S = \left\{\frac{1}{8}ax + \frac{1}{15}\beta^2\right\}/\left\{1 - \frac{T^{-1}}{5}\right\} \quad (49)$$

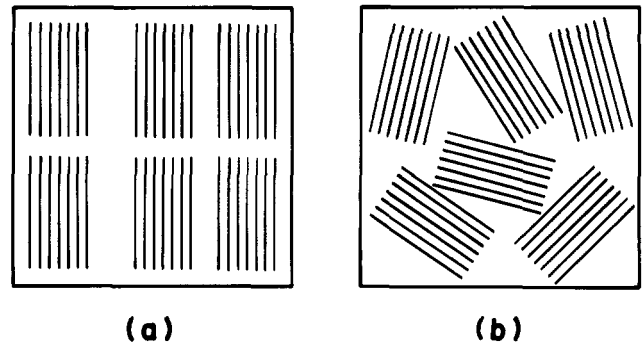

Figure 2. (a) Kuhn segments oriented in the preferred direction of the film specimen. (b) Preferred orientation of Kuhn segments within each domain. The domains are oriented randomly within the film specimen in an undrawn state.

To facilitate understanding of the difference between the system of Erman et al.[5,6] and the present system, two schematic diagrams are proposed in Figure 2 for an extremely high orientational system of segments. Model a is based on Erman's treatment, while model b is associated with our treatment representing a random orientation of domains in which segments in each domain are oriented predominantly with respect to each preferred axis to satisfy the free energy minimum. Following Erman et al.,[5] the preferred axis is fixed in a stable phase whose free energy is at a minimum with respect to the distribution of orientation. They carried out numerical calculations for a thermal and undeformed system in the case of chains consisting of m = 20 segments to check the dependence of the excess free energy with respect to the isotropic state on the normalized disorientation index. According to their results, the excess energy of the anisotropic phase gradually decreases and equates to that of the isotropic phase at x = 6.42, indicating the axial ratio for the first-order phase transition from the isotropic to the anisotropic state, as the asymmetry of the Kuhn segments gets larger. The calculation indicated that, for $x > 6.42$, the free energy of the anisotropic phase is less than that of the isotropic one and the anisotropic phase is the most stable phase. Actually, the second-order orientation factor was almost unity at $x > 10$, indicating almost perfect orientation of rods.

In the present model system, the preferred axis is set in each domain and the orientational degree of the segments becomes pronounced with increasing x, and this tendency is exactly the same as in Erman's model.[5] However, the domains are oriented randomly within a specimen in the undeformed state for all values of x. That is, the most stable anisotropic phase can be realized in each domain and all the unknown parameters β, y/x, and S satisfy the free energy minimum in each domain. The present model means that the equilibrium condition can be realized in each domain, and the boundary regions behave like a sort of energy barrier to hamper uniform orientation of segments within a film in an undeformed state. Thus, this model is thought to be more realistic, since no preferential orientation of segments has ever been observed for a polymer film without applying external stress. For rigid chain polymers, domains with local orientation of segments have been observed under optical microscopy (cross-polarized) for liquid crystals[19] and polymer films.[20]

Results and Discussions

Application to Poly(ethylene terephthalate). Amorphous poly(ethylene terephthalate) (PET) is a good

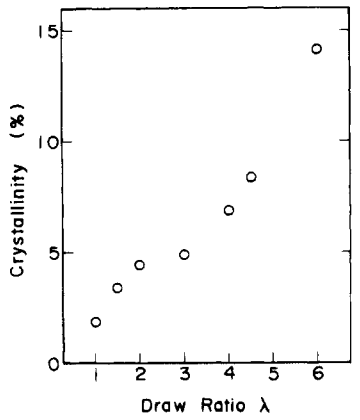

Figure 3. Crystallinity against draw ratio λ for stretched PET specimens.

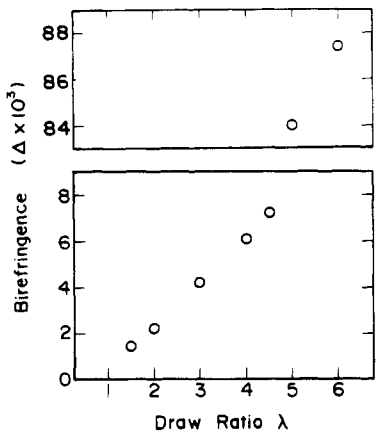

Figure 4. Birefringence against draw ratio λ for stretched PET specimens.

specimen to examine the lattice model for segmental orientation, since the lower crystallinity of the original films can be maintained by elongation in a hot water bath whose temperature is higher than the glass temperature T_g. To check the effect of swelling, the weight of specimens in dried and swollen states was measured. The volume fraction v_2 of polymers was about 0.95.

Figure 3 shows crystallinity as a function of draw ratio λ for specimens stretched in a hot water bath at 90 °C. The increase in crystallinity was very small, being less than 7% at $\lambda < 4$, indicating restriction of strain-induced crystallization.

Figures 4 and 5 show the change in birefringence and the corresponding second-order orientation factor (open circles). The birefringence shows a small increase up to $\lambda = 4$, but a drastic increase was observed beyond $\lambda = 5$, reflecting oriented crystallization. The second-order orientation factor up to $\lambda = 4$ was calculated by neglecting the birefringence of the crystalline phase.[10] The degree of orientation of amorphous chain segments shows a gradual small increase with the draw ratio but is close to zero, indicating an almost random orientation.

Because of lower crystallinity, the orientation of amorphous chain segments was also estimated by X-ray diffraction in terms of the orientation distribution function using specimens drawn up to $\lambda = 4$. Figure 6 shows examples of X-ray diffraction intensity distribution as a function of twice the Bragg angle $2\theta_B$ at $\alpha = 0°$ (upper side) and $\alpha = 90°$ (lower side), in which $\alpha = 0°$ corresponds to the case when the stretching direction is parallel to the vertical axis. The solid circles were obtained after correction for absorption and polarization.

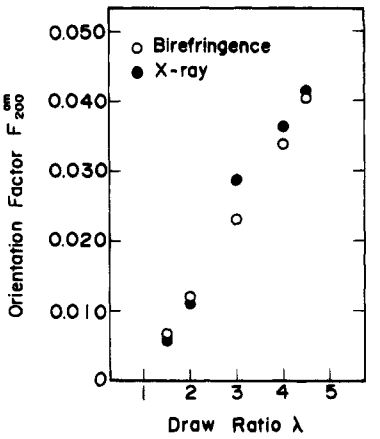

Figure 5. Second-order orientation factor against draw ratio λ for stretched PET specimens. The measurements were done by birefringence (open circles) and X-ray diffraction (solid circles).

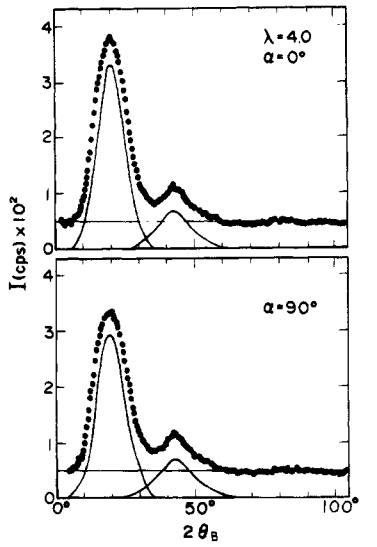

Figure 6. X-ray diffraction intensity distribution of a PET specimen at $\lambda = 4$, measured at $\alpha = 0$ and 90°.

The solid line shows the amorphous contribution after subtracting air scattering. To estimate the orientation distribution function, the first main peak was employed. The X-ray diffraction intensity shown in Figure 6 was measured at 2–5° intervals of α from 0 to 90° by rotating about the film normal direction.

Considering the geometrical arrangement, the angle θ between the amorphous chain axis and the stretching direction is equal to α. Thus, the orientation distribution function can be given by

$$4\pi^2\omega_{am}(\cos\theta) = \frac{\int_{\theta_1}^{\theta_2} I_{am}(\theta,\theta_B)\,d\theta}{\int_0^{\pi}\int_{\theta_1}^{\theta_2} I_{am}(\theta,\theta_B)\,d\theta_B \sin\theta\,d\theta} \quad (50)$$

where $I_{am}(\theta,\theta_B)$ is the scattered intensity distribution from the amorphous phase and θ_1 and θ_2 correspond to the Bragg angles at lower and higher sides of the base of the intensity curve, respectively.

Figure 7 shows the observed orientation distribution function of amorphous chain segments (solid circles) compared with theoretical curves obtained from eq 40 on the basis of the orientation factors F_{l00} calculated by eq 18, in which solid and dashed curves correspond to $x = 1$ and 5, respectively, at a fixed value of $m = 100$.

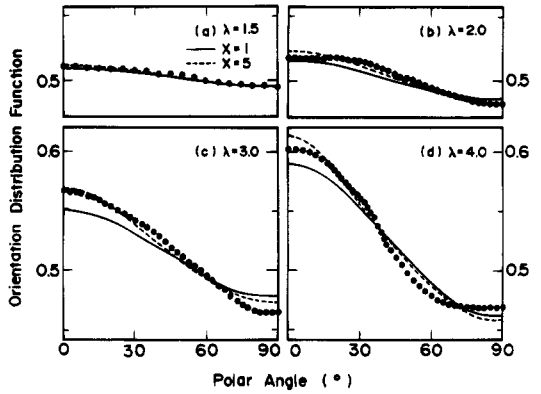

Figure 7. Orientation distribution function of amorphous chain segments of PET with the indicated draw ratio.

With increasing λ, the orientation distribution function becomes sharper. Incidentally, each value (solid circles) of the second-order orientation factor F_{200} calculated from the orientation function in Figure 7 is almost equal to that estimated by birefringence measurements as shown in Figure 5. The orientation function becomes sharper with increasing m. When $m = 100$, the curve at each draw ratio gives the best fit with the experimental plots. In contrast, the curve was hardly affected by the length-to-width ratio x, particularly at draw ratios $\lambda < 2.0$. The best fit, however, was realized at $x = 5$, indicating small improvement. As discussed by Erman,[5] large values of x have a significant effect on the molecular orientation when the thermotropic effect represented by eq 43 is taken into consideration.[6] Although the introduction of this effect is suitable for cross-linked polyester with aromatic groups, the application to the amorphous PET films is undoubtedly meaningless.

Application to Oriented Crystallization of Polyethylene. It is of interest to use the lattice model for studying the effects of amorphous chain segments on the orientation of crystallites by induced crystallization. This concept proposed by Ziabicki et al.[21-23] is due to the fact that the crystallization of amorphous chain segments depends on their orientation. In this paper, the lattice model is applied to their concept. In doing so, the intensity distribution was measured as a function of $2\theta_B$ at a given rotational angle θ_j, and corrections were made for air scattering, background noise, polarization, absorption, incoherent scattering, and amorphous contributions. The intensity curve thus obtained was assumed to be due to the contribution of the crystalline phase. The intensity curve $I_{cry}(\theta_B,\theta_j)$ was separated into the contribution for the individual crystal planes, assuming each peak had a symmetric form. By use of the same process at a given angle θ_j in the range from 0 and 90°, the intensity can be determined for the respective jth crystal plane (j = (110), (200), ...) and the orientation distribution of the jth lattice vector is given by

$$2\pi q_j(\cos\theta_j) = \frac{\int_{\theta_1}^{\theta_2} I_{cry}(\theta_B,\theta_j)\, d\theta_B}{\int_0^{\pi/2}\int_{\theta_1}^{\theta_2} I_{cry}(\theta_B,\theta_j)\, d\theta_B \sin\theta_j\, d\theta_j} \quad (51)$$

Following Hashimoto et al.,[21] the orientation of the c-axes, $W_c(\theta)$, was defined as a kinetically determined crystal orientation distribution function proportional to a normalized distribution of clusters with critical size r^* and l^*, which is given by

$$W_c(\theta) = \text{Const} \times \omega_{am}(\cos\theta) \exp\left[-\frac{\Delta F(r^*,l^*,\theta)}{kT}\right] \quad (52)$$

In eq 52, the free energy for formation of a cylindrical cluster is given by

$$\Delta F(r,l,\theta) = 2\pi r^2\sigma_e + 2\pi rl\sigma_s + \pi r^2 l[\Delta f - (kT/v_0)\ln\chi(\theta)] \quad (53)$$

where σ_e and σ_s are end and side surface free energies having values of 6.75×10^{-6} and 1.3×10^{-6} J/cm^2, respectively, for PE[24] and Δf is the bulk free energy of crystallization. v_0 is the volume of a single element. Considering the free energy $\Delta F(r^*,l^*,\theta)$ associated with a cluster with critical dimensions corresponding to the saddle point, eq 52 can be rewritten as

$$W_c(\theta) = C\omega_{am}(\cos\theta)\exp[-8\pi\sigma_e\sigma_s^2/D(\theta)^2 kT] \quad (54)$$

where C is a normalization constant and the orientation-dependent function $D(\theta)$ is obtained by using $\omega_{am}(\cos\theta)$ in eq 40 as follows:

$$\begin{aligned} D(\theta) &= \Delta f - (kT/v_0)\ln\chi(\theta) \\ &= \Delta f - (kT/v_0)\ln[4\pi\omega_{am}(\cos\theta)] \end{aligned} \quad (55)$$

Assuming Kuhn–Grun statistics for segment orientation, we have

$$\Delta f = \Delta f|_{\lambda=1} - (kT/2N_s v_0)(\lambda^2 + 2/\lambda - 3) \quad (56)$$

A complete description of crystallite orientation may be specified by using three Euler angles, ϕ, θ, and η. The angles ϕ and θ, which define the orientation of the c-axis within the space, are the polar and azimuthal angles, respectively, and η specifies the rotation of the crystal unit around the c-axis. Under uniaxial orientation, the orientation function is independent of ϕ.[25] Using this condition, the orientation distribution function of crystallites is assumed to be as follow:

$$\begin{aligned} \omega(\theta,\eta) = {} & \\ & K_0 W_c(\theta)\{1 + \sigma_1(\lambda-1)\sin^{2(JA-1)}\theta\cos^{2(JC-1)}\eta + \\ & \sigma_2(\lambda-1)(\sin\theta\cos\theta)^{2(JB-1)}\cos^{2(JD-1)}\eta + \\ & \sigma_3(\lambda-1)\cos^{2(JE-1)}\eta + \sigma_4(\lambda-1)\cos^{2(JF-1)}\eta \end{aligned} \quad (57)$$

where K_0 is a normalized constant. The second and third terms on the right-hand side represent the rotation of crystallites around the c-axis which has significant effects at $\theta = 90$ and 45°, respectively. With increasing value of JA and JB, the possibility of the rotation becomes higher. The fourth and fifth terms denote the rotation independent of the polar angle θ. The parameters σ_1, σ_2, σ_3, and σ_4 denote the ease of the rotations, and JC, JD, JE, and JF, the sharpness. The number of the terms on the right-hand side in eq 57 is limited to a maximum of five terms in order to assure the simplicity of the physical meaning of the equation.

As was discussed in the previous paper,[25] the orientation distribution factor F_{l00} of the reciprocal lattice vector of the jth crystal plane can be obtained as follows:

$$F_{l0n} = \int_0^{2\pi}\int_0^{\pi} \omega(\theta,\eta)\, P_l^n(\cos\theta)\cos n\eta \sin\theta\, d\theta\, d\eta \quad (58)$$

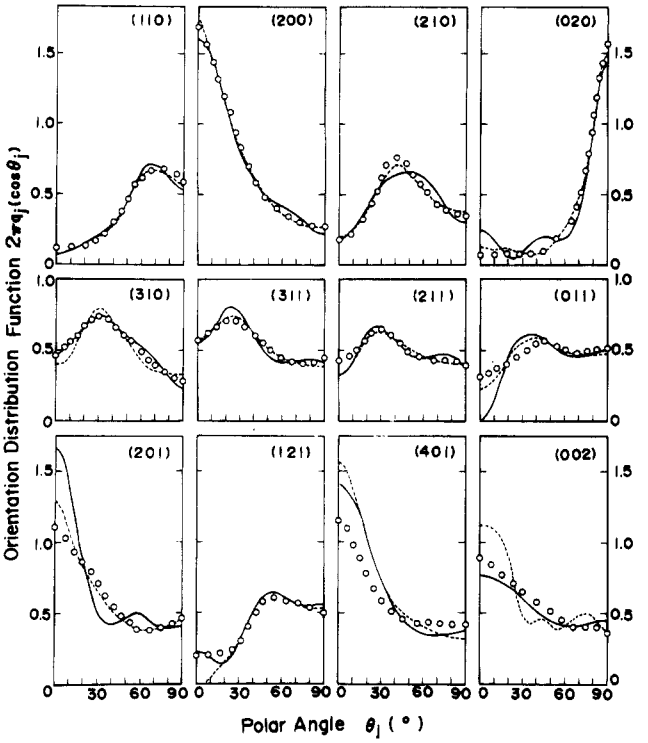

Figure 8. Orientation distribution functions $2\pi q_j(\cos\theta_j)$ of the reciprocal lattice vectors of the indicated crystal planes of PE with $\lambda = 1.5$. Circles: values of $2\pi q_j(\cos\theta_j)$ obtained from experimental measurements. Solid curves: $2\pi q_j(\cos\theta_j)$ calculated from eq 57 (l up to 8). Dashed curves: $2\pi q_j(\cos\theta_j)$ calculated with the 21-term series (l up to 20) with the use of reconstructed F^j_{l0}.

$$F^j_{l0} = F_{l00}P^n_l(\cos\Theta_j) + 2\sum_{n=2}^{l}\frac{(l-n)!}{(l+n)!}F_{l00}P^n_l(\cos\Theta_j)\cos n\varphi_j \quad (59)$$

where Θ_j and Φ_j are the polar and azimuthal angles specifying the orientation of the reciprocal lattice vector with respect to the Cartesian coordinate of a crystal unit. Thus, the orientation distribution function $2\pi q_j(\cos\theta_j)$ of the reciprocal lattice vector may be obtained by substituting eq 59 into the following equation.

$$2\pi q_j(\cos\theta_j) = {}^1/_2 + 2\sum_{l=2}^{\infty}\frac{2l+1}{2}F^j_{l0}P(\cos\theta_j) \quad (60)$$

In numerical calculations, the following values of parameters were used: enthalpy of melting per mole of statistical segments, 4.02 kJ/mol;[26] melting temperature, 137.5 °C;[26] and number of statistical segments, $m = 20$, according to Erman et al.[5] The volume of a single kinetic element, v_0, is an unknown parameter, but the results calculated by eq 60 were found to be insensitive to its value in the range 2×10^{-22}–4×10^{-22} cm^3 at $m = 20$. Accordingly, we adopted 3×10^{-22} cm^3, similar to the value of rubber.[27]

Figures 8 and 9 compare the observed orientation distribution functions $2\pi q_j(\cos\theta_j)$ (open circles) with theoretical distribution functions (solid circles) calculated on the basis of the lattice model and for an original calendered film and a drawn film, respectively. The numerical calculation was continued until the best fit was achieved within the capacity of the simplex method[28]

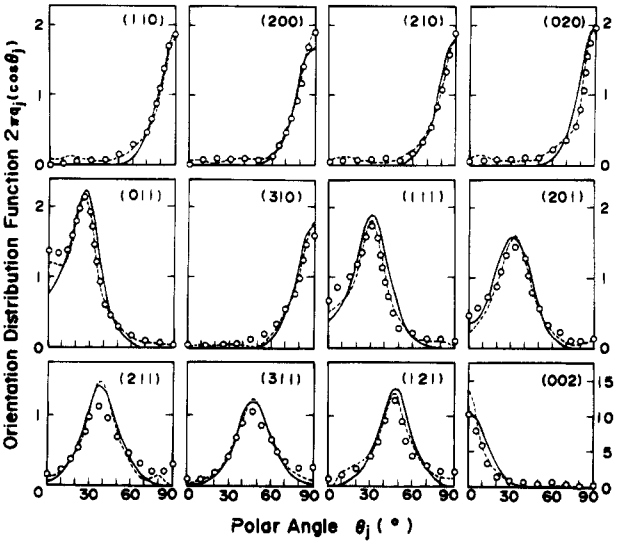

Figure 9. Orientation distribution functions $2\pi q_j(\cos\theta_j)$ of the reciprocal lattice vectors of the indicated crystal planes of PE with $\lambda = 4.0$. Circles: values of $2\pi q_j(\cos\theta_j)$ obtained from experimental measurements. Solid curves: $2\pi q_j(\cos\theta_j)$ calculated from eq 57 (l up to 8). Dashed curves: $2\pi q_j(\cos\theta_j)$ calculated with the 21-term series (l up to 20) with the use of reconstructed F^j_{l0}.

which is a direct method to obtain the object function on the basis of trial and error. The following parameters to give the best fit are obtained: for Figure 8, $\sigma_1 = 13.60$, $\sigma_2 = 3.32$, $\sigma_3 = 1.32$, $\sigma_4 = 11.02$, JA = 9, JB = 5, JC = 5, JD = 1, JE = 8, and JF = 9; for Figure 9, $\sigma_1 = 4.65$, $\sigma_2 = 3.40$, $\sigma_3 = 1.73$, $\sigma_4 = 5.78$, JA = 2, JB = 3, JC = 3, JD = 5, JE = 3, and JF = 1. These parameters indicate that the crystallites exhibit complicated rotational modes in the process of the preferential orientation of the c-axes with respect to the stretching direction. In spite of the expansion of eq 30 with l limited to 8, fairly good agreement between the observed and calculated distribution functions was obtained, even for the less accurately superimposed crystal planes with lower diffraction intensity.

For comparison with the above results, it is important to obtain the orientation distribution function of crystallites $\omega(\theta,\eta)$ according to the method of Roe and Krigbaum.[15] In doing so, the orientation factor F^j_{l0} was obtained from the following equation by using eq 51.

$$F^j_{l0} = \langle P_l(\cos\theta_j)\rangle = \int_0^\pi q_j(\cos\theta_j)P_l(\cos\theta_j)\sin\theta_j\,d\theta_j \quad (61)$$

Substituting the experimental value of F^j_{l0} into eq 61, the coefficient F_{l00} can be determined by solving the linear equations of eq 59. The values of the weighting factors ϱ_j, required in the least-squares calculation, were assigned somewhat subjectively on the basis of the concept that the X-ray diffraction intensity is dependent upon the structure factor of each crystal plane.[14,15] Hence, in this calculation, a weight factor ϱ_j as a first approximation was assumed to be almost proportional to the structure factor and was subsequently modified to obtain the best fit between experimental and calculated results through numerical calculations by computer. By use of the final values of the parameters, a mean-square error between the calculated F^j_{l0} and recalculated F^j_{l0} was obtained.[18]

$$R = \frac{\sum_j \sum_l \varrho_j [(F^j_{l0})_{cal} - (F^j_{l0})_{recal}]^2}{\sum_j \sum_l [(F^j_{l0})_{cal}]^2} \quad (62)$$

The values of R were calculated by using the values of ϱ_j. Figures 8 and 9 show the results (dotted curve) calculated by the method of Roe and Krigbaum for the original and drawn films. To obtain the solid curves, we calculated the best value of F^j_{l0} from eq 59 to minimize the value of R. After that, we recalculated F^j_{l0}, in turn, from the values of F_{l00} and further calculated $2\pi q_j(\cos\theta_j)$ from the recalculated F^j_{l0} value by using eq 60. The values of R for calculating the dashed curves in Figures 8 and 9 were about 8.5% and 9.0%, respectively. Good agreement between the observed and calculated distribution was obtained. Furthermore, the calculated $2\pi q_j(\cos\theta_j)$ are also in good agreement with the theoretical ones calculated by the lattice model.

The orientation distribution functions of crystallites $\omega(\theta,\eta)$ can be calculated by using F_{l00}, assuring the lowest value of R as follows:

$$\omega(\theta,\eta) = {}^1/_2 + 2\sum_{l=2} \frac{2l+1}{2}\left[F_{l00}\,P_l(\cos\theta) + 2\sum_{n=2} \frac{(l-n)!}{(l+n)!} F_{l0n} P^m_l(\cos\theta)\cos n\eta\right] \quad (63)$$

In eq 63, l is limited to 20. Parts a and b of Figure 10 show respectively the orientation distribution functions of crystallites $\omega(\theta,\eta)$ for the original and drawn films as obtained by the application of eq 63. The distribution functions calculated from eq 57 derived by the lattice model also showed almost equivalent profiles to those shown in parts a and b of Figure 10. It is seen that a highly populated region appeared at $\theta = 90°$, $\eta = 0°$ and $\theta = 35°$, $\eta = 0°$ for the original film. The region of $\theta = 90°$, $\eta = 0°$ is related to the second term on the right-hand side of eq 57, while the region of $\theta = 35°$, $\eta = 0°$ can be realized by the summation of the rest of the terms. In the region of $\eta > 40°$, $\theta > 20°$, the distribution function shows a complicated profile. Such a profile was also observed in the distribution function represented by eq 57, although the term taking the complicated distribution is not formulated. The appearance is probably attributed to the summation of the five terms in eq 57. The density, however, is much lower than that at the region at $\eta < 40°$, and therefore the physical meaning can be neglected.

Part b shows a typical profile of the fiber structure. A populated region exists at $\theta = 0°$, and the distribution function is almost independent of η. At $\theta > 50°$, there exist several negative regions and the distribution function shows a complicated profile. Such a complicated distribution is thought to be due to artifacts associated with the inaccuracy of the recalculated F^j_{l0} value as well as with the series termination errors of spherical harmonics. Namely, the appearance of the negative regions is due to the procedure of expanding each sharp distribution function of $2\pi q_j(\cos\theta_j)$ in Figure 10 into a series of spherical harmonics with l limited to 20. This is an expected deficiency of this method. Incidentally, the same negative regions also appeared for the distribution function calculated by using eq 57, since the orientation distribution function $\omega_{am}(\cos\theta)$ of amorphous chain segments contained in $W_c(\theta)$ (see eq 54) is achieved by the expansion into a series of spherical harmonics with l limited to 8.

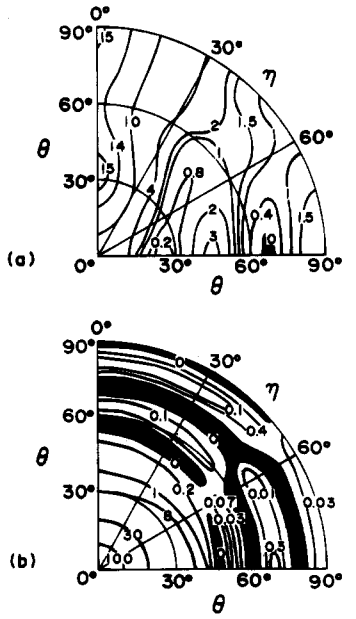

Figure 10. Orientation distribution functions of PE crystallites $\omega(\theta,\eta)$ calculated with the 21-term series (l up to 20) with the use of reconstructed F^j_{l0}: (a) $\lambda = 1.5$; (b) $\lambda = 4.0$.

Returning of Figure 8, it is seen that the orientation distribution function of the a-axes within the calendered film with $\lambda = 1.5$ has a maximum density in the machine direction in spite of the preferential orientation of the c-axes in the same direction. This orientational behavior of the a-axes seems unusual, since the a- and b-axes are perpendicular to the c-axis within a polyethylene unit cell. Actually, the a-axes for the specimen with further elongaiton to $\lambda = 4.0$ are oriented predominantly perpendicular to the machine direction shown in Figure 9. Nevertheless, such drastic orientational change of the a-axes can be realized by the change in the orientation distribution function of crystallites from diagram a to b in Figure 10. Incidentally, the further elongation of the specimen with $\lambda = 1.5$ realized a draw ratio of 14 times, indicating the total draw ratio of 21 times (1.5 × 14). The corresponding Young's modulus was 15.3 GPa. This value is somewhat higher than the value (9 GPa) of drawn melt films (the maximum draw ratio of 13 times) which were prepared with the same powder.

Here it should be noted that the oriented crystallization shown in diagrams a and b in Figure 10 can be determined from the free energy for a cyrindrical cluster associated with the orientation distribution function of deformed polymeric networks calculated on the basis of the lattice model in Figure 1. Accordingly, the good agreement between the experimental and calculated results shown in Figures 7–9 indicates that the application of the lattice model to the elongation of films can successfully explain the detailed molecular orientation of amorphous chain segments of PET and the orientation of crystallites in PE films under induced crystallization by elongation.

Conclusion

Two main conclusions can be drawn.

First, in order to derive a theoretical equation for the orientation of amorphous chain segments, it is important to introduced a modified lattice model. The model

proposed by Erman et al. was modified in this paper. According to the model proposed by Erman et al.,[5,6] the amorphous chain segments are oriented to the preferred (stretching) direction without any elongation, when the length-to-width ratio of each chain segment increased beyond the critical value. In this case, the Helmholtz free energy of the anisotropic phase is less than that of the isotropic phase. In spite of rigorous treatment in terms of the free energy, such behavior has never been observed for polymer films. Such an unfavorable situation is due to the direct introduction of the lattice model proposed by Flory et al.[7,8] for the system of dispersed hard rods. To resolve this discrepancy, the preferred axis associated with the preferential orientation of amorphous chain segments is chosen along the direction between two successive cross-link points and the preferred axis is assumed to deform in an affine fashion. Based on the above concept, the orientation of amorphous chain segments was formulated in terms of the distribution function with respect to the stretching direction by using the Legendre addition theorem.

Secondly, as an application of the proposed model, numerical calculations were carried out to analyze the mechanism of the orientation of amorphous chain segments in drawn PET and the orientation of crystallites of PE under crystallization induced by elongation. For PET, the calculated and experimental results are in good agreement, if suitable values are chosen for the number of amorphous chain segments and their length-to-width ratio. For PE, the orientation distribution function of crystallites was calculated for a calendered film and a drawn film on the basis of the lattice model. The calculated orientation distribution functions $2\pi q_j(\cos\theta_j)$ of the reciprocal lattice vector were in good agreement with the observed ones. The numerical calculations indicate that the orientation of the c-axes depends on that of amorphous chain segments and the orientation behavior of crystallites is strongly affected by their rotation around the c-axis.

Acknowledgment. M.M. expresses his gratitude to Professors Erman and Bahar of Bogazici University of Turkey, who originated the application of lattice model to polymer films, when he visited their laboratory. He also thanks the Natural Science and Engineering of Research Council of Canada and the Japan Society for Promotion of Science, which provided him with a research grant for an extended visit at McGill University which made possible this joint study.

References and Notes

(1) Kuhn, W.; Grun, F. *Kolloid-Z.* **1942**, *101*, 248.
(2) Treloer, L. R. *Trans. Faraday Soc.* **1954**, *50*, 881.
(3) Di Marzio, E. A. *J. Chem. Phys.* **1962**, *36*, 1563.
(4) Tanaka, T.; Allen, G. *Macromolecules* **1977**, *10*, 426.
(5) Erman, B.; Bahar, I.; Kloczkowski, A.; Mark, J. E. *Macromolecules* **1990**, *23*, 5335.
(6) Bahar, I.; Erman, B.; Kloczkowski, A.; Mark, J. E. *Macromolecules* **1990**, *23*, 5341.
(7) Flory, P. J. *Proc. R. Soc. London, Ser. A* **1954**, *234*, 73.
(8) Flory, P. J.; Ronca, G. *Mol. Cryst. Liq. Cryst.* **1979**, *54*, 289 and 311.
(9) Yoon, D.; Flory, P. J. *J. Chem. Phys.* **1974**, *61*, 5366.
(10) Sawatari, C.; Matsuo, M. *Text. Res. J.* **1985**, *55*, 547.
(11) deDaubeny, R.; Bunn, C. W.; Brown, C. *Proc. R. Soc. London, Ser. A* **1954**, *226*, 531.
(12) Bunn, C. W. *Trans. Faraday Soc.* **1939**, *35*, 482.
(13) Matsuo, M.; Sawatari, C. *Macromolecules* **1986**, *19*, 2036.
(14) Roe, R. J.; Krigbaum, W. R. *J. Chem. Phys.* **1964**, *40*, 2608.
(15) Krigbaum, W. R.; Roe, R. J. *J. Chem. Phys.* **1964**, *41*, 737.
(16) Roe, R. J.; Krigbaum, W. R. *J. Appl. Phys.* **1964**, *35*, 2215.
(17) Matsuo, M.; Ozaki, F.; Kurita, H.; Sugawara, S.; Ogita, T. *Macromolecules* **1980**, *13*, 1187.
(18) Matsuo, M.; Sawatari, C.; Iwai, Y.; Ozaki, F. *Macromolecules* **1990**, *23*, 3266.
(19) Matsuo, M.; Kakei, K.; Nagaoka, Y.; Ozaki, F.; Murai, M.; Ogita, T. *J. Chem. Phys.* **1981**, *75*, 5911.
(20) Sawatari, C.; Muranaka, T.; Matsuo, M. *Polym. J.* **1983**, *15*, 33.
(21) Ziabicki, A.; Jarecki, L. *Colloid Polym. Sci.* **1978**, *256*, 332.
(22) Kosc, M.; Ziabicki, A. *Macromolecules* **1982**, *15*, 1507.
(23) Hashimoto, T.; Saijo, K.; Kosc, M.; Kawai, H.; Wasiak, A.; Ziabicki, A. *Macromolecules* **1985**, *18*, 472.
(24) Hoffman, J. D.; Lauritzen, J. I.; Passaglia, E., Jr.; Ross, G. S.; Frolen, L. J.; Weeks, J. J. *Kolloid Z. Z. Polym.* **1969**, *231*, 564.
(25) Matsuo, M.; Hirota, K.; Fujita, K.; Kawai, H. *Macromolecules* **1978**, *11*, 1000.
(26) Mandelkern, L. *Crystallization of Polymer*; McGraw-Hill: New York, 1964.
(27) Hoffman, J. D.; Davies, G. T.; Lauritzen, J., Jr. *Treatise Solid State Chem.* **1976**, 3.
(28) Spendly, W.; Hext, G. R.; Himsworth, F. R. *Technometrics* **1962**, *4*, 441.

MA946285F